



Identification of lithium-ion physics-based model parameter values

锂离子基于物理的模型参数值辨识

Ryan Jobman, M. Scott Trimboli, and Gregory L. Plett*

Department of Electrical and Computer Engineering, University of Colorado Colorado Springs, Colorado Springs, CO 80918, USA

gplett@uccs.edu

Accepted for publication on 10 January 2015

Abstract - Physics-based lithium-ion cell models are a promising alternative to equivalent-circuit models for future battery management systems. However, they also have many more parameter values that must be measured or inferred to make the model match the behaviors of a real cell. This “system identification” problem is significant, and in the past has relied on cell teardown and complex and costly electrochemical experiments to determine the required parameter values.

In this paper, we propose a methodology that minimizes the need for cell teardown and any accompanying electrochemical experimentation. Instead, the model equations are reformulated, and specific cell-level laboratory tests are crafted such that the current–voltage response isolates certain sets of parameter values in the model. These tests are executed on standard cell cycling equipment. Simple and fast optimization procedures then compute the parameter values directly from the specialized lab-test data.

We present results based on a virtual (simulated) cell, where “truth” values for the electrochemical parameters are known for comparison purposes. In most cases, the identified parameters have relative identification error less than 1%.

Keywords - physics-based model; lithium-ion model; measuring lithium-ion model parameters; system identification

I. INTRODUCTION

Battery management systems require cell models to estimate state of charge, state of health, available energy and power. Presently, due to their computational simplicity and robustness, equivalent-circuit models (ECMs) are very widely used [1]. These models execute quickly and have relatively few parameter values to optimize to make the model calculations fit laboratory current–voltage cell-test data. However, ECMs lack the predictive capability of physics-based models (PBMs). For example, while

equivalent-circuit models can predict a cell’s current–voltage behaviors well, they cannot predict internal cell electrochemical variables such as lithium concentrations or electric potentials at different spatial locations internal to the cell. Knowledge of these internal variables is critical to being able to predict and control the instigators of premature aging or unsafe operating conditions.

Physics-based models [2] present possible opportunities to control cells to slow aging [3–4]. But, they come with a cost. One challenge when using PBMs is their computational complexity, but reduced-order models (ROMs) overcome this concern [5–8]. Another challenge is that PBMs also have many more parameter values that must be measured or inferred to make the model equations match the behaviors of a real lithium-ion cell. This “system identification” problem is significant, and in the past has been done either:

1) By the cell builders, who know the materials and related values because they chose them in their design, or

2) By cell teardown and electrochemical and physical tests designed to measure specific parameter values. This option is costly and requires operators having a high level of training. Further, measured parameter values sometimes differ significantly depending on the measurement techniques used and it is not necessarily possible to measure all needed parameter values, so some must be fit by optimizing model predictions to current–voltage data collected from the cell.

More recently, Forman et al. reported work done to use cell current–voltage data to identify these parameter values [9]. In their work, they found that they could identify many but not all parameters of a PBM. This paper presented an important advance in the field—it showed that (at least many of the) parameters can be identified from current–voltage data—but

the method was not very practical since it took a supercomputing cluster 3 weeks to solve the optimizations.

In this paper, we propose a new approach to PBM parameter identification that significantly reduces the number of electrochemical tests that must be performed. If electrode materials are unknown, a cell teardown is still needed to find electrode open-circuit potential (OCP) relationships. Otherwise, no teardown is necessary and simple cell-level laboratory tests are run to isolate groups of parameters in the model to identify their values. Once data are collected, the required CPU time for optimization is several minutes on a desktop computer versus weeks on a supercomputer. This, combined with a suitable ROM, makes PBMs accessible for practical BMS.

We proceed by first reformulating the PBM in terms of new dimensionless grouped parameters. The original set of parameters is not completely observable from the current–voltage data, but the grouped parameters are. This set of grouped parameters is sufficient to be able to simulate all cell electrochemical variables, so the simplified model does not lose generality. The reformulation also removes the need to identify 11 parameter values, which significantly simplifies the system-identification problem. If the full original set of parameters is needed for some reason, a cell teardown can supply the missing dimensions relatively easily.

Next, we will describe cell tests to determine the cell static OCP relationships. Then, we present a way to use pulse tests to identify the majority of the PBM parameters. Finally, we show how to use electrochemical impedance spectroscopy (EIS) to find the remaining values.

We present results based on a virtual (simulated) cell, where “truth” values for the electrochemical parameters are known for comparison purposes. The virtual cell’s coupled PDE model is simulated using COMSOL and the same set of experiments that would be executed in a laboratory. The current–voltage data from the simulation are used to identify the cell’s parameter values: these identified values are compared to the known “truth” values. In most cases, the identified parameters have relative error less than 1%.

II. REFORMULATING THE PDE MODEL

2.1. ORIGINAL PDE MODEL

We assume a standard Doyle–Fuller–Newman pseudo-2d model of a lithium-ion battery cell. This model is derived in detail in [8] and is reviewed here. It comprises four partial-differential equations (PDEs) describing electrical potential and concentrations of lithium in both the solid and electrolyte, plus one algebraic equation describing lithium flux density from solid to electrolyte. The PDEs have boundary conditions at the cell edges and/or junctions between cell regions. In the following, 1d spatial location $x = 0$ is the location of the negative-electrode current collector, $x = L^{\text{neg}}$ is the negative-electrode/separators boundary, $x = L^{\text{neg}} + L^{\text{sep}}$ is the separator/positive-electrode boundary, and $x = L^{\text{tot}} = L^{\text{neg}} + L^{\text{sep}} + L^{\text{pos}}$ is the location of the positive-electrode current collector.

1d radial location $r = 0$ is at a particle center and $r = R_s$ is at the surface of a particle.

Potential in the solid active materials at any point in the negative and positive electrodes $\phi_s(x, t)$ in V is defined by the following PDE and associated boundary conditions:

$$\begin{aligned} \frac{\partial}{\partial x} \sigma_{\text{eff}} \frac{\partial}{\partial x} \phi_s - a_s F j &= 0 \\ \frac{\partial}{\partial x} \phi_s \Big|_{x=L^{\text{neg}}} &= \frac{\partial}{\partial x} \phi_s \Big|_{x=L^{\text{neg}}+L^{\text{sep}}} = 0 \\ \frac{\partial}{\partial x} \phi_s \Big|_{x=0} &= \frac{\partial}{\partial x} \phi_s \Big|_{x=L^{\text{tot}}} = -\frac{i_{\text{app}}}{A \sigma_{\text{eff}}}. \end{aligned}$$

In these equations, σ_{eff} is the effective electronic conductivity of the solid matrix in S m^{-1} and a_s is the specific interfacial surface area of the solid particles in $\text{m}^2 \text{m}^{-3}$ (equivalently, in m^{-1}).

Potential in the electrolyte $\phi_e(x, t)$ in V at any point in the cell is defined by the following PDE and associated boundary conditions:

$$\begin{aligned} \frac{\partial}{\partial x} \left(\kappa_{\text{eff}} \frac{\partial}{\partial x} \phi_e + \kappa_{D,\text{eff}} \frac{\partial}{\partial x} \ln c_e \right) + a_s F j &= 0 \\ \kappa_{\text{eff}} \frac{\partial}{\partial x} \phi_e + \kappa_{D,\text{eff}} \frac{\partial}{\partial x} \ln c_e \Big|_{x=0} &= 0 \\ \kappa_{\text{eff}} \frac{\partial}{\partial x} \phi_e + \kappa_{D,\text{eff}} \frac{\partial}{\partial x} \ln c_e \Big|_{x=L^{\text{tot}}} &= 0. \end{aligned}$$

Here, κ_{eff} is the effective ionic conductivity of the electrolyte in the porous media in S m^{-1} , and t_+^0 is the unitless transference number of the lithium ions with respect to the solvent in the electrolyte. These equations use the shorthand

$$\kappa_{D,\text{eff}} = \frac{2RT(t_+^0 - 1)}{F} \kappa_{\text{eff}},$$

so $\kappa_{D,\text{eff}}$ is not really a free parameter once all other parameters are known.

Lithium concentration in the solid active materials $c_s(x, r, t)$ in mol m^{-3} at any point in the negative and positive electrodes is defined by the following PDE and associated boundary conditions:

$$\begin{aligned} \frac{\partial c_s}{\partial t} &= \frac{1}{r^2} \frac{\partial}{\partial r} \left(D_s r^2 \frac{\partial c_s}{\partial r} \right) \\ D_s \frac{\partial c_s}{\partial r} \Big|_{r=R_s} &= -j \quad \text{and} \quad D_s \frac{\partial c_s}{\partial r} \Big|_{r=0} = 0. \end{aligned}$$

Here, D_s is the diffusivity of lithium in the solid in $\text{m}^2 \text{s}^{-1}$.

Lithium concentration in the electrolyte $c_e(x, t)$ in mol m^{-3} at any point in the cell is defined by the following PDE and associated boundary conditions:

$$\begin{aligned} \frac{\partial (\varepsilon_e c_e)}{\partial t} &= \frac{\partial}{\partial x} D_{e,\text{eff}} \frac{\partial}{\partial x} c_e + a_s (1 - t_+^0) j \\ \frac{\partial c_e}{\partial x} \Big|_{x=0} &= 0 \quad \text{and} \quad \frac{\partial c_e}{\partial x} \Big|_{x=L^{\text{tot}}} = 0. \end{aligned}$$

Here, $D_{e,\text{eff}}$ is the effective diffusivity of the lithium ion in the electrolyte in the porous media, in $\text{m}^2 \text{s}^{-1}$, and ε_e is the unitless volume fraction of the electrolyte in the porous media (also known as the porosity of the media).

Finally, lithium flux density from the solid active materials $j(x,t)$ in $\text{mol m}^{-2} \text{s}^{-1}$ to the electrolyte at any point in the negative and positive electrodes is defined by the following algebraic equation:

$$j = k_0(c_e)^{1-\alpha}(c_{s,\text{max}} - c_{s,e})^{1-\alpha}(c_{s,e})^\alpha \times \left\{ \exp\left(\frac{(1-\alpha)F}{RT}\eta\right) - \exp\left(\frac{-\alpha F}{RT}\eta\right) \right\}$$

$$\eta = \phi_s - \phi_e - U_{\text{ocp}}(c_{s,e}) - FR_{\text{film}}j.$$

In these equations, k_0 is a reaction-rate constant, $c_{s,e}$ is the concentration of lithium at the particle surface, $c_{s,\text{max}}$ is the concentration of lithium in the solid when all lithium sites are occupied, R_{film} is the resistivity of a surface film in Ωm^2 and U_{ocp} is the open-circuit-potential function of the active materials, in V.

Initial concentration of lithium in the electrolyte is denoted by $c_{e,0}$. Initial concentration of lithium in the solid active materials is determined from cell state of charge z via

$$c_{s,0} = c_{s,\text{max}}(\theta_0 + z(\theta_{100} - \theta_0)).$$

Here, θ_0 is the unitless electrode stoichiometry when the cell is at 0% state of charge and θ_{100} is the stoichiometry when the cell is at 100% state of charge.

Table I lists the complete set of parameters that are required if one wishes to simulate the PDE model. (The ordering of parameters in the table is the same order with which they were introduced in this section.) Further, one also needs to know the open-circuit potential (OCP) functions for the two electrode active materials. A total of 35 values must be identified, plus the two OCP functions.

2.2. REFORMULATED PDE MODEL

A close examination of the PDE model reveals that a number of the PBM parameters never appear in isolation but always appear in groups. For example, κ_{eff} is always multiplied by current-collector plate area A and divided by cell-region length L in every equation in which it appears. Therefore, we can make a lumped parameter κ_{tot} that combines these three values into a single parameter. When we do this for all such groups of parameters, neither A nor L appear by themselves in any of the remaining equations. This means that they, as well as several other individual parameters, are not uniquely observable from current–voltage data. So we must reformulate the PDE model in terms of grouped parameters that can be observed from current–voltage data. When we do so, we find that the resulting grouped parameters are dimensionless.

We begin by defining a dimensionless spatial variable \bar{x} such that $0 \leq \bar{x} \leq 1$ in the negative electrode, $1 \leq \bar{x} \leq 2$ in the separator, and $2 \leq \bar{x} \leq 3$ in the positive electrode:

TABLE I, LIST OF PARAMETERS FOR ORIGINAL PDE MODEL

Negative electrode	Separator	Positive electrode
$\sigma_{\text{eff}}^{\text{neg}}$		$\sigma_{\text{eff}}^{\text{pos}}$
a_s^{neg}		a_s^{pos}
L^{neg}	L^{sep}	L^{pos}
A		
$\kappa_{\text{eff}}^{\text{neg}}$	$\kappa_{\text{eff}}^{\text{sep}}$	$\kappa_{\text{eff}}^{\text{pos}}$
D_s^{neg}		D_s^{pos}
R_s^{neg}		R_s^{pos}
$\varepsilon_e^{\text{neg}}$	$\varepsilon_e^{\text{sep}}$	$\varepsilon_e^{\text{pos}}$
$D_{e,\text{eff}}^{\text{neg}}$	$D_{e,\text{eff}}^{\text{sep}}$	$D_{e,\text{eff}}^{\text{pos}}$
t_+^0		
k_0^{neg}		k_0^{pos}
$c_{s,\text{max}}^{\text{neg}}$		$c_{s,\text{max}}^{\text{pos}}$
α^{neg}		α^{pos}
$R_{\text{film}}^{\text{neg}}$		$R_{\text{film}}^{\text{pos}}$
$c_{e,0}$		
θ_0^{neg}		θ_0^{pos}
$\theta_{100}^{\text{neg}}$		$\theta_{100}^{\text{pos}}$

$$\bar{x} = \begin{cases} x/L^{\text{neg}} & 0 \leq x \leq L^{\text{neg}} \\ \frac{x-L^{\text{neg}}}{L^{\text{sep}}} & L^{\text{neg}} \leq x \leq L^{\text{neg}} + L^{\text{sep}} \\ \frac{x-L^{\text{neg}}-L^{\text{sep}}}{L^{\text{pos}}} & L^{\text{neg}} + L^{\text{sep}} \leq x \leq L^{\text{pos}}. \end{cases}$$

Similarly, we define a dimensionless radial variable $\bar{r} = r/R_s$ such that $0 \leq \bar{r} \leq 1$.

Next, we define “total” grouped parameters:

$$\sigma_{\text{tot}} = \frac{\sigma_{\text{eff}}A}{L}, \quad \kappa_{\text{tot}} = \frac{\kappa_{\text{eff}}A}{L}, \quad \kappa_{D,\text{tot}} = \frac{\kappa_{D,\text{eff}}A}{L},$$

$$D_{s,\text{tot}} = \frac{D_s}{R_s^2}, \quad D_{e,\text{mod}} = \frac{D_{e,\text{eff}}Ac_{e,0}}{L(1-t_+^0)^2}, \quad R_{\text{film,tot}} = \frac{R_{\text{film}}}{a_sAL},$$

$$k_{\text{step}} = \frac{a_s k_0 \sqrt{c_{e,0}}}{\varepsilon_s}, \quad L_{e,\text{mod}} = \frac{\varepsilon_e AL c_{e,0}}{(1-t_+^0)^2}.$$

We also define new electrochemical variables:

$$j_{\text{tot}} = a_s AL j,$$

$$n_s = a_s AL R_s c_s / 3,$$

$$c_{e,\text{ratio}} = c_e / c_{e,0}.$$

These new parameter and electrochemical-variable definitions allow us to reformulate the PDE model.

Electrical potential in the solid active materials at any point in the negative and positive electrodes is now defined by the following PDE and associated boundary conditions:

$$\sigma_{\text{tot}} \frac{\partial^2}{\partial \bar{x}^2} \phi_s - F j_{\text{tot}} = 0$$

$$\left. \frac{\partial}{\partial \bar{x}} \phi_s \right|_{\bar{x}=1} = \left. \frac{\partial}{\partial \bar{x}} \phi_s \right|_{\bar{x}=2} = 0$$

$$\left. \frac{\partial}{\partial \bar{x}} \phi_s \right|_{x=0} = \left. \frac{\partial}{\partial \bar{x}} \phi_s \right|_{\bar{x}=3} = -\frac{i_{\text{app}}}{\sigma_{\text{tot}}}.$$

TABLE II, LIST OF PARAMETERS FOR REFORMULATED PDE MODEL

Negative electrode	Separator	Positive electrode
$\sigma_{\text{tot}}^{\text{neg}}$		$\sigma_{\text{tot}}^{\text{pos}}$
$\kappa_{\text{tot}}^{\text{neg}}$	$\kappa_{\text{tot}}^{\text{sep}}$	$\kappa_{\text{tot}}^{\text{pos}}$
$D_{s,\text{tot}}^{\text{neg}}$		$D_{s,\text{tot}}^{\text{pos}}$
V_e^{neg}	V_e^{sep}	V_e^{pos}
$D_{e,\text{tot}}^{\text{neg}}$	$D_{e,\text{tot}}^{\text{sep}}$	$D_{e,\text{tot}}^{\text{pos}}$
t_+^0		
$k_{\text{step}}^{\text{neg}}$		$k_{\text{step}}^{\text{pos}}$
$n_{s,\text{max}}^{\text{neg}}$		$n_{s,\text{max}}^{\text{pos}}$
$R_{\text{film,tot}}^{\text{neg}}$		$R_{\text{film,tot}}^{\text{pos}}$
θ_0^{neg}		θ_0^{pos}
$\theta_{100}^{\text{neg}}$		$\theta_{100}^{\text{pos}}$

Electrical potential in the electrolyte at any point in the cell is now defined by the following PDE and associated boundary conditions:

$$\begin{aligned} \kappa_{\text{tot}} \frac{\partial^2}{\partial \bar{x}^2} \phi_e + \kappa_{D,\text{tot}} \frac{\partial^2}{\partial \bar{x}^2} \ln c_{e,\text{ratio}} + F j_{\text{tot}} &= 0 \\ \kappa_{\text{tot}} \frac{\partial}{\partial \bar{x}} \phi_e + \kappa_{D,\text{tot}} \frac{\partial}{\partial \bar{x}} \ln c_{e,\text{ratio}} \Big|_{\bar{x}=0} &= 0 \\ \kappa_{\text{tot}} \frac{\partial}{\partial \bar{x}} \phi_e + \kappa_{D,\text{tot}} \frac{\partial}{\partial \bar{x}} \ln c_{e,\text{ratio}} \Big|_{\bar{x}=3} &= 0. \end{aligned}$$

Normalized lithium concentration in the solid active materials at any point in the negative and positive electrodes is now defined by the following PDE and associated boundary conditions:

$$\begin{aligned} \frac{\partial n_s}{\partial t} &= \frac{1}{\bar{r}^2} \frac{\partial}{\partial \bar{r}} \left(D_{s,\text{tot}} \bar{r}^2 \frac{\partial n_s}{\partial \bar{r}} \right) \\ D_{s,\text{tot}} \frac{\partial n_s}{\partial \bar{r}} \Big|_{\bar{r}=1} &= -j_{\text{tot}} \\ D_{s,\text{tot}} \frac{\partial n_s}{\partial \bar{r}} \Big|_{\bar{r}=0} &= 0. \end{aligned}$$

Normalized lithium concentration in the electrolyte at any point in the cell is now defined by the following PDE and associated boundary conditions:

$$\begin{aligned} L_{e,\text{mod}} \frac{\partial c_{e,\text{ratio}}}{\partial t} &= \frac{\partial}{\partial \bar{x}} D_{e,\text{mod}} \frac{\partial}{\partial \bar{x}} c_{e,\text{ratio}} + \frac{1}{1-t_+^0} j_{\text{tot}} \\ \frac{\partial c_{e,\text{ratio}}}{\partial \bar{x}} \Big|_{\bar{x}=0} &= 0 \\ \frac{\partial c_{e,\text{ratio}}}{\partial \bar{x}} \Big|_{\bar{x}=3} &= 0. \end{aligned}$$

Finally, lithium flux density from the solid active materials to the electrolyte at any point in either electrode is now defined by the following algebraic equation:

$$\begin{aligned} j_{\text{tot}} &= 2j_{0,\text{tot}} \sinh \left(\frac{F}{2RT} \eta \right) \\ j_{0,\text{tot}} &= k_{\text{step}} \sqrt{c_{e,\text{ratio}}} \sqrt{n_{s,\text{max}} - n_{s,e}} \sqrt{n_{s,e}} \\ \eta &= \phi_s - \phi_e - U_{\text{ocp}}(n_{s,e}) - FR_{\text{film,tot}} j_{\text{tot}}. \end{aligned}$$

In this equation, we have assumed that $\alpha = 0.5$, which is common in the literature.

Initial normalized concentration of lithium in the electrolyte is denoted by $c_{e,\text{ratio}} = 1$. Initial normalized concentration of lithium in either electrode's solid active materials is determined from cell state of charge z via

$$n_{s,0} = n_{s,\text{max}} (\theta_0 + z(\theta_{100} - \theta_0)).$$

Table II lists the complete set of parameters that is required if one wishes to simulate the reformulated PDE model. (The ordering of parameters in the table is the same as in Table I, except that the reformulation removes some parameters from the model.) We also still need to know the OCP functions for the two electrode active materials. A total of 24 values must be identified, plus the two OCP functions. The reformulation has removed the requirement for finding 11 parameter values—a greater than 25% reduction.

With this reformulated model, we are still able to simulate the potential in the solid and electrolyte and the concentration of lithium in the electrolyte exactly; further, we are able to simulate the concentration of lithium in the solid as well as the lithium flux density to within scaling factors. If we are required to simulate these latter two quantities exactly, then we still require a cell teardown to measure a_s , A , L , and R_s . These geometric properties are relatively easy to measure using SEM imaging. However, we often don't need the exact values of these variables: knowing them to within a scaling factor is sufficient when computing power limits based on lithium depletion, for example.

III. OPEN-CIRCUIT VOLTAGE TESTS

We identify the model parameter values and functions using specialized laboratory tests that isolate groups of parameters. Equilibrium (thermodynamic) properties are found using pseudo-static open-circuit voltage tests; instantaneous (resistive) properties are found using pulse tests; and intermediate-frequency properties are found using electrochemical impedance spectroscopy (EIS) tests. These tests, and the parameters that are identified by them, are discussed in the following sections.

3.1. WHEN THE ELECTRODE CHEMISTRIES ARE KNOWN

The open-circuit potential relationships $U_{\text{ocp}}(n_s)$ for both electrodes are needed in order to compute the overpotential η in the model equations. Further, we require $n_{s,\text{max}}$, θ_0 , and θ_{100} for both electrode materials to initialize a simulation.

If the electrode chemistries are known, then some of these parameter values are available from the literature. The OCP functions $U_{\text{ocp}}(\theta)$ will be known, and we can compute $\theta = n_s/n_{s,\text{max}}$ if we are able to determine $n_{s,\text{max}}$. Therefore, we need only find $n_{s,\text{max}}$, θ_0 and θ_{100} for both electrodes.

To do so, we first charge the battery cell to 100% SOC to initialize the OCV test. The test begins by very slowly discharging the cell down to 0% SOC. (The desire is for the cell to be in a pseudo-equilibrium condition at all times;

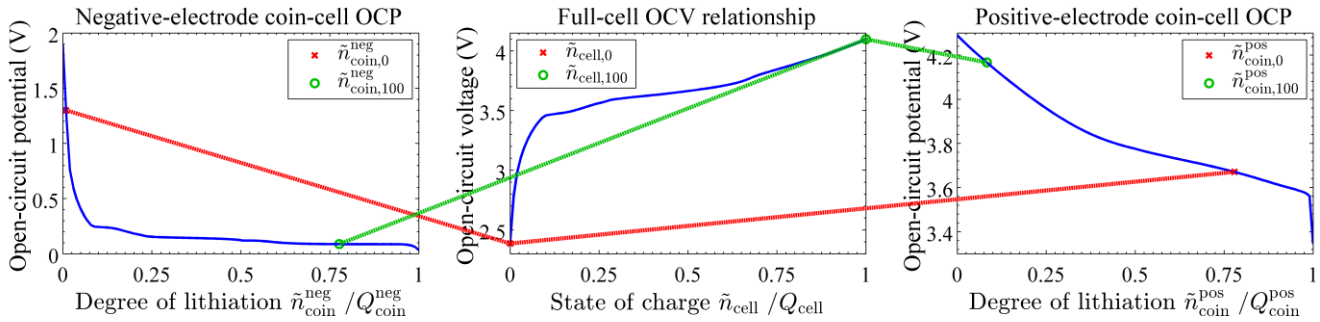


Fig. 1, Example showing relationship between electrode coin-cell OCP functions and cell OCV function.

however, that would require infinitely long test duration. A good compromise is a discharge rate of about C/30.) Then, the cell is very slowly recharged to 100% SOC. Voltage and net ampere-hours discharged at every point in the test are recorded. Cell open-circuit voltage can be approximated as the average of the charge and discharge voltages at every SOC during the test.

When the cell is at 100% SOC, then both electrodes will have stoichiometry equal to their respective θ_{100} values. Similarly, when the cell is at 0% SOC, then both electrodes will be at their respective θ_0 values. At every point in the test, the OCV is equal to the OCP of the positive electrode minus the OCP of the negative electrode at the present electrode θ values. To find θ_0 and θ_{100} for both electrodes, we perform a nonlinear optimization that matches the cell OCV curve with the difference between electrode OCP curves. The optimization is initialized with guesses for θ_0 and θ_{100} for both electrodes; then, these four values are adjusted to better match the OCV to the OCP curves. In MATLAB®, the `lsqnonlin` function from its Optimization Toolbox™ can be used, for example. This optimization takes on the order of a few seconds to complete.

Cell total capacity (in mol) is equal to

$$Q = n_{s,\max} |\theta_{100} - \theta_0|.$$

So, once we have optimized the θ values, we can use the maximum discharged capacity Q from the OCV test and the θ values to determine the values of $n_{s,\max}$ for each electrode.

3.2. WHEN THE ELECTRODE CHEMISTRIES ARE UNKNOWN

Different steps are required if the electrode chemistries are unknown. We are not aware of any way to avoid a minimal cell teardown in this case.

To find the needed functions and parameters, the cell is opened and coin cells are made of negative-electrode active materials versus lithium metal and positive-electrode active materials versus lithium metal. The same discharge/charge test as was outlined in Sect. 3.1 is performed on these coin cells (in addition to the full cell). However, for the coin cells, we don't know a priori the voltage limits for the electrodes that correspond to 100% and 0% cell SOC. Therefore, we assume some voltage limits and charge *above* the assumed maximum voltage and discharge *below* the assumed minimum voltage to

ensure that the OCP curves that we identify contain the range of stoichiometries that will be needed by the model.

Averaging the discharge and charge voltages for the coin cells at every net ampere-hour point in the test gives us OCP relationships as functions of excess lithiation beyond the (unknown) initial lithiation \vec{n}_{coin} of the coin cell, measured in ampere-hours. (When the coin cells are initially charged to the starting voltage for the OCP test, there is a nonzero unknown amount of lithium present, which must be identified to create an accurate model.) The OCP relationships are not yet functions of stoichiometry θ . Additional steps will be required to convert the OCP relationships to functions of θ .

We convert net ampere-hours discharged in an OCP test to moles discharged, denoted as \vec{n}_{coin} by multiplying by $3600/F$. By optimizing the fit between the cell OCV and the electrode OCP curves, we can find operating points $\vec{n}_{\text{coin},0}$ corresponding to θ_0 and $\vec{n}_{\text{coin},100}$ corresponding to θ_{100} . This is illustrated in Fig. 1, which shows OCP curves for example negative- and positive-electrode materials versus lithium metal, and the OCV curve for the overall cell. It also shows $\vec{n}_{\text{coin},0}$ and $\vec{n}_{\text{coin},100}$ values that optimize the fit between the OCV and OCP curves.

We have not yet found the initial lithiation of the coin cell, \vec{n}_{coin} nor the maximum theoretic capacity of the coin cell, $n_{\text{coin},\max}$. It turns out that we will not need to do so. However, by the end of the pulse test, we will be able to calculate these values from those that have been found, if it is of interest to do so.

In summary, by this point we have determined the general shape of the OCP curves. If the electrode chemistries are known, then we have also found $n_{s,\max}$, θ_0 and θ_{100} for both electrodes. If electrode chemistries are unknown, then we have instead found $\vec{n}_{\text{coin},0}$ and $\vec{n}_{\text{coin},100}$ for both electrodes and still need to find \vec{n}_{coin} and $n_{\text{coin},\max}$ to convert $\vec{n}_{\text{coin},0}$ values into θ values. These remaining values will be found by pulse testing.

IV. PULSE TESTS

The OCV tests isolated the pseudo-static thermodynamic properties of the cell. In contrast, the pulse tests are designed to isolate the instantaneous response of the cell to a pulse of input current. This corresponds to an ohmic resistance term.

In the model, lithium concentrations do not react instantly, so parameters corresponding to the solid and electrolyte

concentration equations are not identified by this test. Parameters corresponding to the lithium flux density and the two electric-potential equations are found instead.

Cell resistance is a function of cell SOC as well as the magnitude of the input current (resistance is nonlinear). These two facts allow us to collect sufficiently rich data to identify the majority of the model parameter values using a simple pulse test.

The test is simple. We first fully charge the cell. Then, the cell is allowed to rest until it reaches equilibrium. Next, a discharge pulse is applied, and the instantaneous change in voltage is recorded. This process is repeated at multiple cell SOC values and with multiple pulse magnitudes. Charge pulses can also be applied, and the instantaneous voltage change recorded. Resistance is then computed as the magnitude of the voltage change divided by the magnitude of the current pulse, and is tabulated versus SOC and rate.

To use these data to find model parameter values, we first formulate cell resistance as closed-form equations in terms of the unknown parameter values. Then we use nonlinear optimization to adjust the unknown values until the predicted resistances match the measured resistances as closely as possible. By the end of this step, we will have identified 15 of the 24 model parameter values, plus the two OCP functions.

4.1. CELL RESISTANCE

We are greatly aided by the reduced-order-model (ROM) equations of Lee et al. when determining cell resistance [6,8]. In Lee's ROM, the cell dynamics were approximated, but the instantaneous response was computed exactly in closed form. Since concentrations (and hence open-circuit potential terms) don't change instantaneously, we can write the immediate change in voltage in response to a pulse input as

$$\lim_{t \rightarrow 0^+} v(t) = F[R_{\text{film,tot}}^{\text{pos}} j_{\text{tot}}^{\text{pos}}(3, t) - R_{\text{film,tot}}^{\text{neg}} j_{\text{tot}}^{\text{neg}}(0, t)] + [\tilde{\phi}_e(3, t)]_1 + [\eta^{\text{pos}}(3, t) - \eta^{\text{neg}}(0, t)].$$

The lithium-flux-density and electrolyte-potential terms are linear, so their limit can be written in terms of Laplace-domain transfer functions as

$$\lim_{t \rightarrow 0^+} v_{\text{lin}}(t) = \lim_{s \rightarrow \infty} F[R_{\text{film,tot}}^{\text{pos}} J_{\text{tot}}^{\text{pos}}(3, s) - R_{\text{film,tot}}^{\text{neg}} J_{\text{tot}}^{\text{neg}}(0, s)] + [\tilde{\phi}_e(3, s)]_1.$$

We will see how to evaluate this expression in Sect. 4.2. The nonlinear terms can be computed by taking the limit of

$$\eta(\bar{x}, t) = \frac{2RT}{F} \operatorname{asinh} \left(\frac{j_{\text{tot}}(\bar{x}, t)}{2j_{0,\text{tot}}} \right)$$

where we will evaluate the instantaneous change in j_{tot} using transfer functions, and where we compute $j_{0,\text{tot}}$ as

$$j_{0,\text{tot}} = k_{\text{step}} \sqrt{c_{e,\text{ratio}}} \sqrt{n_{s,\text{max}} - n_s} \sqrt{n_s}.$$

For the pulse tests, $c_{e,\text{ratio}} = 1$ since the pulse is applied when the cell is in equilibrium. The parameter k_{step} is an unknown to be found by the pulse-test data. If the electrode chemistries are known, then $n_{s,\text{max}}$ was already found as part of the OCV test;

otherwise, it will be optimized as part of the pulse test. In either case, the pulse test will optimize $n_{s,0}$ for both electrodes such that we can compute n_s from cell SOC z and capacity Q as

$$n_s^{\text{neg}} = n_{s,0}^{\text{neg}} + zQ$$

$$n_s^{\text{pos}} = n_{s,0}^{\text{pos}} - zQ.$$

If the electrode chemistries are not known a priori, then the pulse tests will optimize values for both $n_{s,\text{max}}$ and $n_{s,0}$ for both electrodes, where the conversion between full-cell normalized electrode concentrations and coin-cell normalized electrode concentrations is done via:

$$n_s^{\text{neg}} = n_{s,0}^{\text{neg}} + Q \frac{\tilde{n}_{\text{coin}}^{\text{neg}} - \tilde{n}_{\text{coin},0}^{\text{neg}}}{\tilde{n}_{\text{coin},100}^{\text{neg}} - \tilde{n}_{\text{coin},0}^{\text{neg}}}$$

$$n_s^{\text{pos}} = n_{s,0}^{\text{pos}} - Q \frac{\tilde{n}_{\text{coin}}^{\text{pos}} - \tilde{n}_{\text{coin},0}^{\text{pos}}}{\tilde{n}_{\text{coin},100}^{\text{pos}} - \tilde{n}_{\text{coin},0}^{\text{pos}}}.$$

This relationship also allows us to solve for \tilde{n}_{coin} from n_s to look up an OCP value from the coin-cell experiments. It was derived using:

$$\tilde{n}_{\text{coin}}^{\text{neg}} = \tilde{n}_{\text{coin},0}^{\text{neg}} + z(\tilde{n}_{\text{coin},100}^{\text{neg}} - \tilde{n}_{\text{coin},0}^{\text{neg}})$$

$$\tilde{n}_{\text{coin}}^{\text{pos}} = \tilde{n}_{\text{coin},0}^{\text{pos}} - z(\tilde{n}_{\text{coin},100}^{\text{pos}} - \tilde{n}_{\text{coin},0}^{\text{pos}}).$$

Once we have found $n_{s,\text{max}}$ and $n_{s,0}$, we can compute n_s in both electrodes for any cell SOC of interest, and from that we can compute the stoichiometric operating points via $\theta = n_s/n_{s,\text{max}}$. Therefore, we can now compute the OCP curves for both electrodes as functions of θ .

4.2. TRANSFER FUNCTIONS FOR PULSE TESTS

In Lee et al. [6,8], a cell ROM is made by linearizing the PDE model and creating transfer functions of the electrochemical variables. These transfer functions shared a common impedance ratio

$$\nu^2(s) = \frac{\frac{1}{\sigma_{\text{tot}}} + \frac{1}{\kappa_{\text{tot}}}}{R_{s,e,\text{tot}} + \frac{1}{FD_{s,\text{tot}}} \left[\frac{\partial U_{\text{ocp}}}{\partial n_{s,e}} \Big|_{n_{s,0}} \right] \left[\frac{1}{1 - \sqrt{\frac{s}{D_{s,\text{tot}}}} \coth \left(\sqrt{\frac{s}{D_{s,\text{tot}}}} \right)} \right]},$$

where

$$R_{s,e,\text{tot}} = R_{\text{ct,tot}} + R_{\text{film,tot}}.$$

In [6], the charge-transfer resistance was found to be

$$R_{\text{ct,tot}} = \frac{RT}{F^2 j_{0,\text{tot}}},$$

when expressed in reformulated parameters. However, this equation was derived under the assumption that the cell current is small, which is not true for the pulse-testing system-identification step. In [10], Lee derived a different charge-transfer resistance that applies even for large pulses:

$$R_{\text{ct,tot}} = \frac{RT}{F^2 \sqrt{j_{0,\text{tot}}^2 + (i_{\text{app}}/(2F))^2}}.$$

We use this formulation of $R_{\text{ct,tot}}$ in the following.

TABLE III, PARAMETERS FOUND BY END OF PULSE TESTING

Negative electrode	Separator	Positive electrode
$\sigma_{\text{tot}}^{\text{neg}}$		$\sigma_{\text{tot}}^{\text{pos}}$
$\kappa_{\text{tot}}^{\text{neg}}$	$\kappa_{\text{tot}}^{\text{sep}}$	$\kappa_{\text{tot}}^{\text{pos}}$
$k_{\text{step}}^{\text{neg}}$		$k_{\text{step}}^{\text{pos}}$
$n_{s,\text{max}}^{\text{neg}}$		$n_{s,\text{max}}^{\text{pos}}$
$R_{\text{film,tot}}^{\text{neg}}$		$R_{\text{film,tot}}^{\text{pos}}$
θ_0^{neg}		θ_0^{pos}
$\theta_{100}^{\text{neg}}$		$\theta_{100}^{\text{pos}}$

By the initial-value theorem, we will need to find the limit of several transfer functions as s approaches infinity. In the limit, the impedance ratio (square root) becomes

$$\nu_{\infty} = \sqrt{\frac{1}{\kappa_{\text{tot}}} + \frac{1}{\sigma_{\text{tot}}}} \sqrt{\frac{1}{R_{s,e,\text{tot}}}}$$

This will be substituted into the following transfer functions.

The transfer function for lithium flux density in the negative electrode can be written in terms of the reformulated parameters as:

$$\frac{J_{\text{tot}}(z, s)}{I_{\text{app}}(s)} = \nu(s) \frac{\sigma_{\text{tot}} \cosh(\nu(s)z) + \kappa_{\text{tot}} \cosh(\nu(s)(z-1))}{F(\kappa_{\text{tot}} + \sigma_{\text{tot}}) \sinh(\nu(s))},$$

where $z = \bar{x}$ in the negative electrode. In the positive electrode, the transfer function is multiplied by -1 and we substitute $z = 3 - \bar{x}$. When s approaches infinity, we have

$$\frac{J_{\text{tot},\infty}(0)}{I_{\text{app}}(s)} = \frac{\nu_{\infty} (\sigma_{\text{tot}} + \kappa_{\text{tot}} \cosh(\nu_{\infty}))}{F(\kappa_{\text{tot}} + \sigma_{\text{tot}}) \sinh(\nu_{\infty})}$$

at the current-collector locations.

The transfer function for the linear part of the electrolyte potential at the positive-electrode current collector is

$$\begin{aligned} \frac{[\tilde{\Phi}_e(3, s)]_1}{I_{\text{app}}(s)} = & - \frac{((\sigma_{\text{tot}}^{\text{neg}} - \kappa_{\text{tot}}^{\text{neg}}) \tanh(\frac{\nu^{\text{neg}}(s)}{2}))}{\kappa_{\text{tot}}^{\text{neg}} (\kappa_{\text{tot}}^{\text{neg}} + \sigma_{\text{tot}}^{\text{neg}}) \nu^{\text{neg}}(s)} \\ & - \frac{((\sigma_{\text{tot}}^{\text{pos}} - \kappa_{\text{tot}}^{\text{pos}}) \tanh(\frac{\nu^{\text{pos}}(s)}{2}))}{\kappa_{\text{tot}}^{\text{pos}} (\kappa_{\text{tot}}^{\text{pos}} + \sigma_{\text{tot}}^{\text{pos}}) \nu^{\text{pos}}(s)} \\ & - \frac{1}{(\kappa_{\text{tot}}^{\text{neg}} + \sigma_{\text{tot}}^{\text{neg}})} - \frac{1}{\kappa_{\text{tot}}^{\text{sep}}} - \frac{1}{(\kappa_{\text{tot}}^{\text{pos}} + \sigma_{\text{tot}}^{\text{pos}})}. \end{aligned}$$

In the limit as s approaches infinity, this becomes

$$\begin{aligned} \frac{[\tilde{\Phi}_e,\infty(3)]_1}{I_{\text{app}}(s)} = & - \frac{(\sigma_{\text{tot}}^{\text{neg}} - \kappa_{\text{tot}}^{\text{neg}}) \tanh(\frac{\nu_{\infty}^{\text{neg}}}{2})}{\kappa_{\text{tot}}^{\text{neg}} (\kappa_{\text{tot}}^{\text{neg}} + \sigma_{\text{tot}}^{\text{neg}}) \nu_{\infty}^{\text{neg}}} \\ & - \frac{(\sigma_{\text{tot}}^{\text{pos}} - \kappa_{\text{tot}}^{\text{pos}}) \tanh(\frac{\nu_{\infty}^{\text{pos}}}{2})}{\kappa_{\text{tot}}^{\text{pos}} (\kappa_{\text{tot}}^{\text{pos}} + \sigma_{\text{tot}}^{\text{pos}}) \nu_{\infty}^{\text{pos}}} \\ & - \frac{1}{\kappa_{\text{tot}}^{\text{neg}} + \sigma_{\text{tot}}^{\text{neg}}} - \frac{1}{\kappa_{\text{tot}}^{\text{sep}}} - \frac{1}{\kappa_{\text{tot}}^{\text{pos}} + \sigma_{\text{tot}}^{\text{pos}}}. \end{aligned}$$

In summary, pulse-test resistances can be expressed in terms of all parameters found by the OCV tests plus the additional parameters listed in Table III. Optimizing the values in Table III so that predicted resistances match measured resistances at different levels of input current and

cell SOC gives us a little over half of the model parameters. Optimizing this set of parameters takes on the order of tens of seconds using the MATLAB® Optimization Toolbox™.

V. EIS TESTS

The remaining model parameter values may be found via EIS tests. To do so, we measure the frequency response of the cell around different SOC values and optimize the remaining model parameters so the model frequency response matches the measured frequency response as well as possible.

The small-signal transfer function of a cell can be expressed as [8]:

$$\begin{aligned} \frac{\tilde{V}(s)}{I_{\text{app}}(s)} = & FR_{s,e,\text{tot}}^{\text{pos}} \frac{J_{\text{tot}}(3, s)}{I_{\text{app}}(s)} - FR_{s,e,\text{tot}}^{\text{neg}} \frac{J_{\text{tot}}(0, s)}{I_{\text{app}}(s)} + \frac{[\tilde{\Phi}_e(3, s)]_1}{I_{\text{app}}(s)} \\ & + \frac{2RT(1-t_+^0)}{F} \left[\frac{\tilde{C}_{e,\text{ratio}}(3, s)}{I_{\text{app}}(s)} - \frac{\tilde{C}_{e,\text{ratio}}(0, s)}{I_{\text{app}}(s)} \right] \\ & + \left[\frac{\partial U_{\text{ocp}}^{\text{pos}}}{\partial n_{s,e}^{\text{pos}}} \right]_{n_{s,0}^{\text{pos}}} \frac{\tilde{N}_{s,e}^{\text{pos}}(3, s)}{I_{\text{app}}(s)} - \left[\frac{\partial U_{\text{ocp}}^{\text{neg}}}{\partial n_{s,e}^{\text{neg}}} \right]_{n_{s,0}^{\text{neg}}} \frac{\tilde{N}_{s,e}^{\text{neg}}(0, s)}{I_{\text{app}}(s)}. \end{aligned}$$

This can be turned into a frequency response by making the substitution $s = j\omega$. We have already seen transfer functions for the lithium flux density and the linear part of the electrolyte potential. To evaluate this frequency response, we further need transfer functions for the electrolyte concentration ratio and the solid concentration.

The transfer function for solid concentration in the negative electrode can be found to be

$$\begin{aligned} \frac{\tilde{N}_{s,e}(z, s)}{I_{\text{app}}(s)} = & \left[\frac{\sigma_{\text{tot}} \cosh(\nu(s)z) + \kappa_{\text{tot}} \cosh(\nu(s)(z-1))}{3FD_{s,\text{tot}}(\kappa_{\text{tot}} + \sigma_{\text{tot}}) \sinh(\nu(s))} \right] \\ & \times \left[\frac{\nu(s)}{1 - \sqrt{s/D_{s,\text{tot}}} \coth(\sqrt{s/D_{s,\text{tot}}})} \right]. \end{aligned}$$

In the positive electrode, the transfer function is simply multiplied by -1 .

The transfer functions for the electrolyte concentration ratio are quite lengthy, and we don't have room to reproduce them here. They can be found by taking the transfer functions for electrolyte concentration from [6,8], reformulating in terms of the new model parameters, and dividing by $c_{e,0}$. The $(1-t_+^0)$ term in the frequency response is absorbed into the transfer functions such that only the lumped parameters defined to date are needed to express it.

In summary, a cell's frequency response can be expressed in terms of all parameters found by the OCV and pulse tests plus all additional unknown cell parameter values. Optimizing the remaining unknown parameter values such that the predicted frequency response matches the measured frequency response at different cell SOC's give us the complete identified model except for t_+^0 , which is a value that we assume in this work (but, see discussion in Sect. VII, where we mention an additional step that can be used to find this value as well). Optimization of this set of parameters takes on the order of a few minutes using MATLAB®'s Optimization Toolbox™.

TABLE IV. PARAMETERS USED IN SIMULATION

Symbol	Units	Negative electrode	Separator	Positive electrode
L	μm	128	76	190
R_s	μm	12.5	—	8.5
A	m^2	1	1	1
σ	S m^{-1}	100	—	3.8
ε_s	$\text{m}^3 \text{m}^{-3}$	0.471	—	0.297
ε_e	$\text{m}^3 \text{m}^{-3}$	0.357	0.724	0.444
brug	—	1.5	—	1.5
$c_{s,\text{max}}$	mol m^{-3}	26 390	—	22 860
$c_{e,0}$	mol m^{-3}	2 000	2 000	2 000
θ_0	—	0.05	—	0.78
θ_{100}	—	0.53	—	0.17
D_s	$\text{m}^2 \text{s}^{-1}$	3.9×10^{-14}	—	1.0×10^{-13}
D_e	$\text{m}^2 \text{s}^{-1}$	7.5×10^{-11}	7.5×10^{-11}	7.5×10^{-11}
t_+^0	—	0.363	0.363	0.363
k	$\text{mol}^{-1/2} \text{m}^{5/2} \text{s}^{-1}$	1.94×10^{-11}	—	2.16×10^{-11}
α	—	0.5	—	0.5
R_{film}	Ωm^2	0.0	—	—

VI. RESULTS

As a feasibility test of the proposed approach, we implemented the methodology in simulation. This has the advantage that the actual parameter values are known exactly, so identification results can be verified directly. It does have several limitations, however, as discussed in Sect. VII.

The assumed cell parameter values are from [2] and are listed in Table IV. In addition to the parameter values listed in the table, we also model the effective conductivities and diffusivities as

$$\begin{aligned}\sigma_{\text{eff}} &= \sigma \varepsilon_s^{\text{brug}} \\ \kappa_{\text{eff}} &= \kappa \varepsilon_e^{\text{brug}} \\ D_{e,\text{eff}} &= D_e \varepsilon_e^{\text{brug}};\end{aligned}$$

we model the electrolyte conductivity (in S m^{-1}) as

$$\begin{aligned}\kappa(c_e) &= 4.1253 \times 10^{-2} + 5.007 \times 10^{-4} c_e - 4.7212 \times 10^{-7} c_e^2 \\ &\quad + 1.5094 \times 10^{-10} c_e^3 - 1.6018 \times 10^{-14} c_e^4\end{aligned}$$

the negative-electrode OCP in V as

$$U_{\text{ocp}}^{\text{neg}}(\theta) = -0.16 + 1.32 \exp(-3.0\theta) + 10.0 \exp(-2000.0\theta),$$

and the positive-electrode OCP in V as

$$\begin{aligned}U_{\text{ocp}}^{\text{pos}}(\theta) &= 4.19829 + 0.0565661 \tanh(-14.5546\theta + 8.60942) \\ &\quad - 0.0275479 \left[\frac{1}{(0.998432 - \theta)^{0.4924656}} - 1.90111 \right] \\ &\quad - 0.157123 \exp(-0.04738\theta^6) \\ &\quad + 0.810239 \exp[-40(\theta - 0.133875)].\end{aligned}$$

In this case, we assumed that we “knew” the chemistries of the two electrodes, so simply must find the θ values for both electrodes via the OCV tests. These were identified with high precision.

Data for the pulse tests were collected by simulating the FOM in COMSOL Multiphysics for different equilibrium SOC initializations and for different charge and discharge pulse magnitudes. Care had to be taken to add second-order smoothing to the input pulse to avoid problems with simulation convergence. Resistance was measured as the absolute voltage change between the equilibrium voltage and the cell voltage measured shortly after the application of the current pulse (the short delay was necessary to account for the time lag of the second-order smoothing), divided by the input-current pulse magnitude. These data, normalized to the C rate of the cell, are plotted in Fig. 2. We see that cell resistance is a nonlinear function of input-current magnitude and SOC. The fact of this nonlinearity is critical for the pulse testing to be able to extract multiple parameters from the same test. If the resistance were linear, we would not be able to distinguish between the components that comprise its calculation; because it is nonlinear, we are able to do so.

Nonlinear optimization was performed to optimize values for the parameters listed in Table III. Candidate values for these parameters were inserted into the equations that predict cell resistance; these resistances were then compared to the measured resistances of Fig. 2; the candidate values were then adapted to optimize the fit between the predicted and measured resistances. At the end of the optimization, the difference between the measured and predicted resistances was very small (on the order of $\text{n}\Omega$), and is plotted in Fig. 3. Optimized pulse-test parameter values are presented in Table V.

We see that the conductivities were identified very well. The worst-case result was on the order of 2% relative error (σ_{tot} for the negative electrode). The k_{step} parameters were identified with negligible error and the film-resistance values had high *relative* error, but low *absolute* error: the errors were not significant at the output of the model.

Data for the EIS tests were collected using a small-signal reduced-order model [8], although different approaches could have been used (e.g., see [11]). These data are plotted in Figs. 4 and 5. We see some nonlinear variation with respect to SOC, but not nearly as much as for the pulse-test data. (This uniformity limits our ability to identify different parameters in the model uniquely. In a physical cell, we would expect more variation than this.)

Nonetheless, the identification results using this data were quite good. Identified parameter values are listed in Table VI. The biggest challenge at this point is in estimating the lumped electrolyte values $L_{e,\text{mod}}$. All other parameters were estimated well.

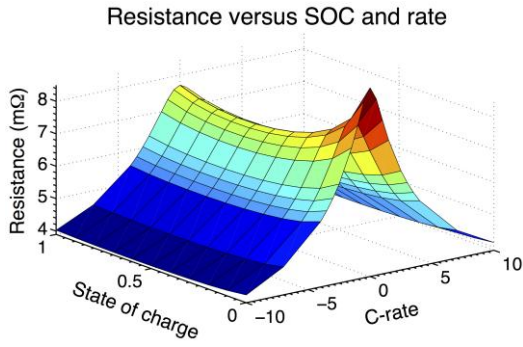


Fig.2, Resistance of Doyle cell.

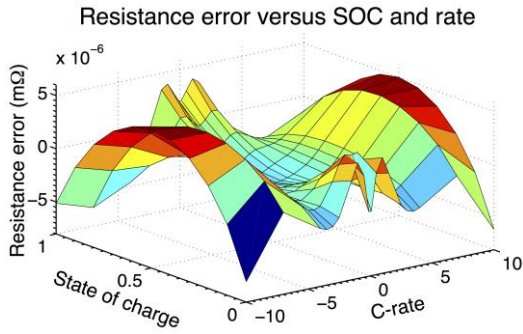


Fig.3, Error in estimates of Doyle-cell resistance.

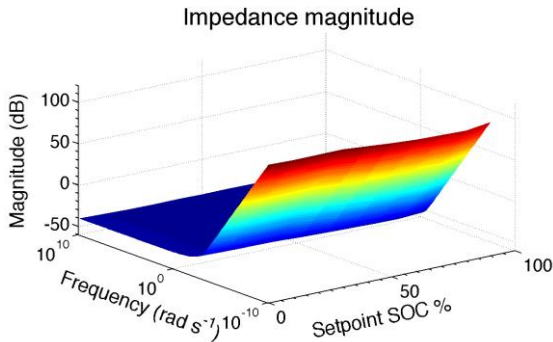


Fig. 4, Doyle-cell impedance magnitude.

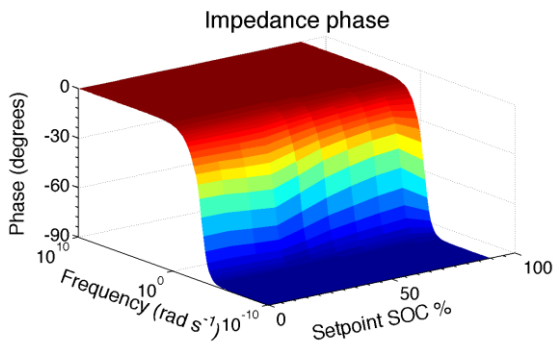


Fig.5, Doyle-cell impedance magnitude.

VII. DISCUSSION

These results have demonstrated that the proposed methodology works quite well in an ideal setting—when the actual cell dynamics exactly match the model of the cell

TABLE V, IDENTIFIED PARAMETERS VIA PULSE TESTS

Symbol	Units	Negative electrode	Separator	Positive electrode
True parameter values				
κ_{tot}	S	175.65	164.12	854.38
σ_{tot}	S	3.680×10^5		5940
$R_{film,tot}$	Ω	0		0
k_{step}	s^{-1}	2.077×10^{-4}		3.408×10^{-4}
Estimated parameter values				
κ_{tot}	S	175.64	164.12	854.46
σ_{tot}	S	3.785×10^5		5944
$R_{film,tot}$	Ω	1.07×10^{-7}		8.60×10^{-11}
k_{step}	s^{-1}	2.077×10^{-4}		3.408×10^{-4}

TABLE VI, IDENTIFIED PARAMETERS VIA EIS TESTS

Symbol	Units	Negative electrode	Separator	Positive electrode
True parameter values				
$D_{s,tot}$	s^{-1}	4.01×10^3		7.23×10^2
$D_{e,mod}$	$mol s^{-1}$	6.16×10^{-4}	3.00×10^{-3}	5.76×10^{-4}
$L_{e,mod}$	mol	2.25×10^{-1}	2.71×10^{-1}	4.16×10^{-1}
t_+^0	—	0.363		
Estimated parameter values				
$D_{s,tot}$	s^{-1}	4.01×10^3		7.23×10^2
$D_{e,mod}$	$mol s^{-1}$	6.13×10^{-4}	2.98×10^{-3}	5.73×10^{-4}
$L_{e,mod}$	mol	2.04×10^{-1}	3.12×10^{-1}	1.94×10^{-1}
t_+^0	—	Assumed to be 0.363		

dynamics, when measurements are noise-free, and when the input to the cell for different tests can be controlled accurately. We have begun to apply this methodology to actual lithium-ion cells and find that the method also works there, albeit with a few caveats.

It turns out there is some difficulty associated with collecting reliable pulse-test data, especially at high pulse-current magnitudes. One possibility is that the equipment used to generate the pulses is not capable of producing ideal Heaviside step functions; in practice, an oscillation is evident in the input current as the cell tester attempts to converge to the commanded current level, which biases the results. Therefore, we use the pulse testing to give only approximate values to the parameters in Table III, but rely on data collected from the subsequent tests to refine the estimates.

Due in part to the difficulty of collecting reliable pulse-test data, we also conduct an additional steady-state resistance test. The additional data is helpful in achieving convergence of

consistent parameter value sets. Further, it allows us to identify t_+^0 and $c_{e,0}$ uniquely.

Additionally, the cell model used in the work presented here did not consider the effects of a double-layer capacitance. It turns out that this capacitance tends to charge and discharge quickly so that from a practical point of view it does not have a large impact on long-term model predictions. Nevertheless, it does significantly change the EIS results at high frequencies. We therefore find it necessary to include the double-layer capacitance in our methodology to identify model parameters for physical cells.

Finally, we do not address error bounds on the identified parameters within this work. We plan to use the methods proposed in [9] to do so in future research. Indeed, results of system ID on physical cells is a topic of planned future publications.

VIII. CONCLUSION

We believe that physics-based models of lithium-ion cells will be required by future battery-management systems in order to optimize the performance/lifetime tradeoff for large battery packs. For this to be practical, we must be able to identify the parameter values of the physics-based models. In the past, manufacturers have been reluctant to disclose this information, so we must find other ways to discover it.

This paper has proposed a methodology that can be used to find physics-based lithium-ion cell-model parameter values. We began by reformulating the equations to eliminate redundant and unobservable dimensional parameters from the model—these parameters are not necessary to being able to simulate the model equations. We then proposed OCV, pulse, and EIS testing to collect data to be used when finding the parameter values. Each test isolated a group of parameters such that the optimizations required to perform the parameter fits was minimized in scope, which makes it quite fast.

If electrode chemistries are known, no cell teardown is needed. The entire system-identification process can be accomplished via cell-level testing only. If electrode chemistries are unknown, a minimal teardown is required to form coin cells from the electrode materials in order to determine OCP data. This is a relatively straightforward and inexpensive task.

We used simulation in this paper to create the data to be used by the methodology so that we could have known “truth” values for all parameters against which to compare results. The identified parameter values agreed with the truth values very well in all cases. For physical cells, we mentioned some additional steps that should be taken to improve on these methods. We plan to publish results for physical cells in the near future.

VIII. DISCLAIMER

The information, data, or work presented herein was funded in part by an agency of the United States Government. Neither

the United States Government nor any agency thereof, nor any of their employees, makes any warranty, express or implied, or assumes any legal liability or responsibility for the accuracy, completeness, or usefulness of any information, apparatus, product, or process disclosed, or represented that its use would not infringe privately owned rights. References herein to any specific commercial product, process, or service by trade name, trademark, manufacturer, or otherwise does not necessarily constitute or imply its endorsement, recommendation, or favoring by the United States Government or any agency thereof. The views and opinions of authors expressed herein do not necessarily state or reflect those of the United States Government or any agency thereof.

IX. ACKNOWLEDGMENT

The information, data, or work presented herein was funded in part by the Advanced Research Projects Agency-Energy (ARPA-E), U.S. Department of Energy, under Award Number DE-AR0000271.

This work used the EAS Data Center or EAS Cloud, which is supported by the College of Engineering and Applied Science, University of Colorado Colorado Springs.

REFERENCES

- [1] X. Hu, S. Li, and H. Peng, “A Comparative Study of Equivalent Circuit Models for Li-ion Batteries,” *Journal of Power Sources*, **198**, 359–367, 2012.
- [2] M. Doyle, J. Newman, A.S. Gozdz, C.N. Schmutz, and J-M Tarascon, “Comparison of Modeling Predictions with Experimental Data from Plastic Lithium Ion Cells,” *J. Electrochem. Soc.*, **143**(6), 1890–1903, 1996.
- [3] K.A. Smith, C.-Y. Wang, “Power and Thermal Characterization of a Lithium-Ion Battery Pack for Hybrid-Electric Vehicles,” *Journal of Power Sources*, **160**, 662–673, 2006.
- [4] G.L. Plett, *Battery Management Systems, Volume II: Equivalent-Circuit Methods*, Artech House, 2016.
- [5] J.L. Lee, A. Chemistruck, and G.L. Plett, “Discrete-Time Realization of Transcendental Impedance Functions, with Application to Modeling Spherical Solid Diffusion,” *Journal of Power Sources*, **206**, 367–377, 2012.
- [6] J.L. Lee, A. Chemistruck, and G.L. Plett, “One-Dimensional Physics-Based Reduced-Order Model of Lithium-Ion Dynamics,” *Journal of Power Sources*, **220**, 430–448, 2012.
- [7] J.L. Lee, L. Aldrich, K. Stetzel, and G.L. Plett, “Extended Operating Range for Reduced-Order Model of Lithium-Ion Cells,” *Journal of Power Sources*, **255**, 85–100, 2014.
- [8] G.L. Plett, *Battery Management Systems, Volume I: Battery Modeling*, Artech House, 2015.
- [9] J.C. Forman, S.J. Moura, J.L. Stein, and H.K. Fathy, “Genetic Identification and Fisher Identifiability Analysis of the Doyle–Fuller–Newman Model from

- Experimental Cycling of a LiFePO₄ Cell,” *Journal of Power Sources*, **210**, 263–275, 2012.
- [10] J.L. Lee, *Reduced-Order Physics-Based Model of Lithium-Ion Batteries*, PhD dissertation, University of Colorado Colorado Springs, Ch. 6, 2012.
- [11] M. Doyle, J.P. Meyers, and J. Newman, “Computer Simulations of the Impedance Response of Lithium Rechargeable Batteries,” *J. Electrochem. Soc.*, **147**, 99–110, 2000.